Collagen–iron oxide nanoparticle based ferrogel: large reversible magnetostrains with potential for bioactuation

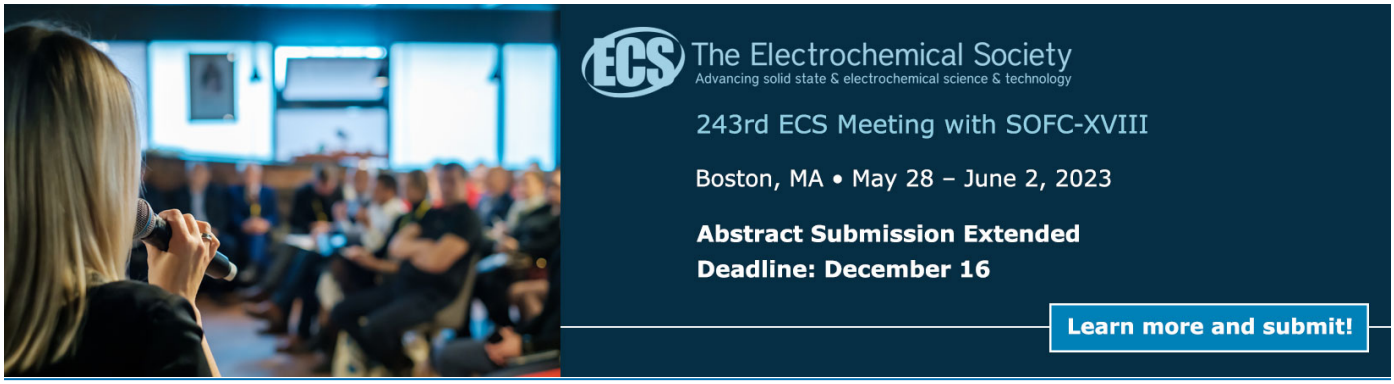

IOP Publishing Multifunct. Mater. 3 (2020) 035001 https://doi.org/10.1088/2399-7532/abaa2d

Multifunctional Materials

OPEN ACCESS

RECEIVED
30 April 2020

REVISED
13 July 2020

ACCEPTED FOR PUBLICATION
28 July 2020

PUBLISHED
25 August 2020

PAPER

Collagen–iron oxide nanoparticle based ferrogel: large reversible magnetostrains with potential for bioactuation

Philine Jauch[1], **Andreas Weidner**[2], **Stefanie Riedel**[1], **Nils Wilharm**[1], **Silvio Dutz**[2] and **Stefan G. Mayr**[1]

[1] Division of Surface Physics, Department of Physics and Earth Sciences, University of Leipzig and Leibniz Institute of Surface Engineering (IOM), Permoserstr. 15, 04318, Leipzig, Germany
[2] Institute of Biomedical Engineering and Informatics (BMTI), Technische Universität Ilmenau, Gustav-Kirchhoff-Str. 2, 98693, Ilmenau, Germany

E-mail: stefan.mayr@iom-leipzig.de

Keywords: collagen, magnetic nanoparticle, ferrogel, magnetic actuator, soft actuator

Abstract

Smart materials such as stimuli responsive polymeric hydrogels offer unique possibilities for tissue engineering and regenerative medicine. As, however, most synthetic polymer systems and their degradation products lack complete biocompatibility and biodegradability, this study aims to synthesize a highly magnetic responsive hydrogel, based on the abundant natural biopolymer collagen. As the main component of vertebratal extracellular matrix, it reveals excellent biocompatibility. In combination with incorporated magnetic iron oxide nanoparticles, a novel smart nano-bio-ferrogel can be designed. While retaining its basic biophysical properties and interaction with living cells, this collagen-nanoparticle hydrogel can be compressed to 38% of its original size and recovers to 95% in suitable magnetic fields. Besides the phenomenology of this scenario, the underlying physical scenarios are also discussed within the framework of network models. The observed reversible peak strains as large as 150% open up possibilities for the fields of biomedical actuation, soft robotics and beyond.

1. Introduction

Contrary to most approaches, which aim to create artificial materials, the focus of this study is to control and utilize a natural biodegradable polymer with promising potential for biomedical applications. By controlling the polymer with defined forces, new insights into mechanical properties can be derived and used for refined modelling approaches of the material. Collagen is the main component of natural vertebratal extracellular matrix [1] and therefore an ideal material to create biocompatible hydrogels for diverse applications such as 3D cell culture [2, 3], extracellular matrix models [4] and scaffolds for tissue engineering [5]. *In vivo* as well as *in vitro* collagen forms complex network structures, driven by self-assembly processes during polymerization. Thereby procollagen triple-helices self-assemble to collagen micro fibrils and finally collagen fibres [6]. The resulting network structure is able to store tremendous amounts of water while remaining mechanical stability. In combination with incorporated coated iron oxide nanoparticles, a new promising magnetic responsive biomaterial can be derived. Iron oxide nanoparticles are characterized—besides their magnetic properties—by superior biocompatibility [7], leading to application in a wide field ranging from engineering to biomedicine [8–10]. For the following investigations, magnetic iron oxide nanoparticles were evenly dispersed and deep-seated in a collagen hydrogel, while the basic properties of collagen were not changed. The resulting material allows a giant magnetic deformation and potential magnetic manipulation, while remaining its biodegradability and mechanical properties. But so far, this strain of a collageneous network could only be achieved through methods like physical pressure and centrifugation [11–13]. These methods lack the option of reversibility and *in vivo* control. Furthermore, due to the partly inhomogeneous force on the collagen network, the sensitive polymer chains can be irreversibly damaged at points of high force. Contrary, pulling the collagen network equally on every point simultaneously, allows an even and gentle compression or elongation force. In this study, the basic properties of collagen with and without

embedded magnetic nanoparticles (MNPs) were compared to determine the influence of the MNPs on the system. Afterwards, collagen hydrogels with incorporated MNPs were placed in a static magnetic field gradient and first compressed and then elongated nearly to their original size. The collected data with defined forces was utilized to model and mathematically explain collagen behaviour on a global scale.

2. Experimental details

2.1. Preparation and characterization of MNPs

The MNPs used within this study were prepared similar to the well-known wet chemical precipitation method [14] changing the alkaline medium to 1.17 M $NaHCO_3$-solution [15]. This solution was added directly under permanent stirring to a $FeCl_2/FeCl_3$-solution with a Fe^{2+}/Fe^{3+}-ratio of 1:1.7. A brownish precipitate occurred and after adding distilled water, the particles were boiled for 5 min at 100 °C. That way, single core MNPs were formed under the release of CO_2 and the colour of the suspension turned black. The obtained MNP suspension was washed twice by magnetic separation with distilled water using a high-performance permanent magnet to remove excess educts and salts.

Coating with diethylaminoehtyl-dextran (DEAE-dextran), resulting in positively charged MNPs, seems to be a promising strategy to stabilise the MNP in water and to obtain a homogeneous MNP distribution within the collagen. Therefore, as prepared MNPs were coated by DEAE as shown before [16]. In short, HCl was added to the suspension of as prepared MNPs to adjust the pH-value at 2 to 3 for short term stabilisation and the MNPs were dispersed by ultra-sonic treatment (Sonopuls GM200, Bandelin electronic, Berlin, Germany) and in an ultra-sonic bath (S100H, Elmasonic, Germany) for 1 min each. At the same time, the DEAE-dextran (Cat. No. 4198.1, Carl Roth GmbH + Co. KG, Germany) was dissolved in distilled water with a mass ratio (coating-core) of 1:1. Under permanent stirring, the MNP suspension was tempered in a water bath to 45 °C, the DEAE solution was steadily added and the dispersion was stirred permanently for further 60 min at 45 °C. Afterwards, it was washed magnetically with distilled water twice using the same method as described before for the raw MNPs to remove excess coating material. To disperse the MNPs again, they have been treated with the same ultra-sonic procedure as mentioned before. Finally, the concentration was adjusted by adding distilled water to its final value.

The zeta potential of the MNPs was determined to be $+28.5 \pm 5.1$ mV and the hydrodynamic diameter d_h (1st peak) $= 170.4 \pm 67.7$ nm. All measurements have been performed by diluting the suspension 1:60 (v/v) and using a Zetasizer (nanoZS, Malvern, UK) with a clear disposable zeta cell (DTS 1070) and appropriate software (Zetasizer Ver. 6.20). Magnetic properties of the prepared samples were determined by means of vibrating sample magnetometry (VSM; Micromag 3900, Princeton Measurement Systems, USA). Table A1 (appendix) summarizes the obtained values. The plain magnetic cores ('powder') show a saturation magnetization M_s which is typical for the magnetic iron oxides and the values for coercivity H_c and relative remanence M_r/M_s confirm a superparamagnetic behaviour of the particles with a negligible hysteresis. The ferrofluids of the MNPs ('fluid') for the preparation of the particle loaded gels have a MNP concentration of about 2.3% by mass. The MNP concentration in the collagen gel ('gel') was determined magnetically to be 0.06% by mass. For the gel, slightly increased H_c and M_r/M_s compared to the values of pure MNPs, indicates a moderate agglomeration of the MNPs within the gel.

2.2. Collagen preparation

The collagen gels were synthesized by mixing rat tail collagen (Collagen R, 0.4% solution, Cat. No. 47256.01; SERVA Electrophoresis, Germany) and bovine skin collagen (Collagen G, 0.4% solution, Cat. No. L 7213; Biochrom, Germany) in a ratio of 1:2, respectively, following the protocol of Kunschmann *et al* [17] and Fischer *et al* [18]. A mixing of rat tail and bovine skin collagen was used because the resulting network strongly resembles human collagenous networks [19, 20]. A phosphate buffer containing Na_2HPO_4 (Cat. No. 71636; Sigma-Aldrich Chemie GmbH, Germany) and NaH_2PO_4 (Cat. No. 71507; Sigma-Aldrich Chemie GmbH) was added to the collagen mixture on ice, to obtain a total phosphate molarity of 200 mM and a pH value of 7.5. For MNP-containing collagen gels, MNPs were added for a final concentration of 0.5 mg ml^{-1} iron oxide before the polymerization started. At 37 °C and 100% humidity, the collagen samples were incubated for 24 h for polymerization. Afterwards, the polymerized samples were rinsed twice with distilled water and stored at room temperature until measured.

2.3. Rheology measurements

Rheology measurements in oscillation were performed with a MCR-300 bulk rheometer (Anton Paar; Austria) with a 10 mm-diameter parallel-plate geometry at a temperature controlled environment of 25 °C.

The collagen samples were cut out of collagen sheets with a diameter of 10 mm and a height of approximately 2 mm. To determine the strain independent region, strain sweeps at 1 Hz were performed (not shown here). Afterwards the storage and loss moduli were measured via frequency sweeps. In the strain independent region (0.01% to 5%) at 1% strain and 1 Hz, the characteristic elastic modulus was identified. To avoid dehydration, only one measurement was performed per sample. The experiment was repeated three times with min. five samples each for collagen with and without incorporated MNPs.

2.4. Network structure analysis

To analyse the network structure, collagen samples were stained with TAMRA (5/6-carboxytetramethylrhodamine succinimidyl ester, 50 μg ml^{-1}, ex./em. wavelength: 540/565 nm, Cat. No. 90022; BIOTREND Chemikalien GmbH, Germany) for 12 h and rinsed twice with distilled water. 3D image stacks were recorded with a confocal laser scanning microscope (CLSM, TCS SP2; Leica Microsystems, Germany) with a helium-neon laser (wavelength 543 nm) and binarized. Afterwards, the 3D euclidean distances to the nearest fibre were determined for every voxel and a corresponding distance map with the local maxima representing the centre of a pore was created. Similar to Mickel *et al* [21], the euclidean distance of the local maximum correlates to the pore size of that pore. From all individual pore sizes, the mean of the distribution was received, as already performed in Riedel and Hietschold *et al* [22]. The significance was tested by an independent two-sample t-test.

2.5. Cellular viability

As described in detail in Riedel and Hietschold *et al* [22], NIH/3T3 (CRL-1658; ATCC, Germany) fibroblasts were cultivated on collagen hydrogels for 72 h at 37 °C and 100% humidity and harvested by collagen dissolution using collagenase A (3 mg ml^{-1}, Cat. No.10103578001; Sigma-Aldrich Chemie GmbH). A propidium-iodide and annexin V staining (V13242; Thermofischer) was added according to manufacturer's recommendations and analysed using the flow cytometer LSR Fortessa II (BD Biosciences, USA) and the data was analysed using Flowing Software (Perttu Terho, Flowing Software, 2018). The experiment was repeated three times and the data is shown in the appendix in figure 1.

2.6. Magnetic deformation

The collagen samples with a measured concentration of 0.06% iron oxide per mass were placed in the magnetic field gradient of an electromagnet (Art.No. 700046, Schueler Magnetic Ltd., Germany) as shown in figure 1, operated with a power supply from Delta Elektronika (Art.No. SM 120–25 D, Netherlands) and regulated by LabVIEW (National Instruments Germany GmbH, Germany). To determine the magnetic field gradient, measurements with a hall effect sensor were performed (Art. No. SPE 670, Schwille Elektronik Produktions- und Vertriebs GmbH, Germany) and shown in figure 1(c). The deformation was filmed with an industrial camera (Art.No. UI-3240ML, IDS Imaging Development Systems GmbH, Germany, Art. No. HF16HA-1B, Fujifilm Holdings Corporation, Japan) in combination with uEye-software (IDS Imaging Development Systems GmbH, Germany). After approximately 19 h, compression was applied by reversing the direction of the magnetic force via turning over the sample. The deformation curve and maximum deformation were determined via image analysis and a self-written python software, as described in detail by Wilharm *et al* [23]. The magnetization curve for the collagen gel is shown in figure 1(d).

3. Experimental results

In the first type of experiments, we were able to show, that the MNPs did not influence the polymerization or mechanical characteristics of collagen hydrogels. Since the MNPs are added before the polymerization process starts to ensure a homogenous distribution, it was important to demonstrate, that the typical network structure still can be achieved under slightly modified conditions. Therefore, stained collagen networks with and without MNPs were investigated by confocal laser-scanning microscopy and compared (figures 2(a)–(d)). With these images, pore size analysis was performed as described in detail in the experimental section. The results (3.1 $\pm$ 0.4 μm for collagen without MNPs, 3.4 $\pm$ 1.2 μm with MNPs) show no significant influence of the MNPs on the pore sizes. Both, network structure and pore size remain similar and are consistent with previous published values for collagen networks [22, 24]. Furthermore, rheology measurements were performed with the hydrogels to investigate the mechanical impact of the MNPs on the network. No significant difference between collagen hydrogels with and without MNPs could be detected. The storage modulus (24.2 $\pm$ 15.9 Pa for collagen without MNPs, 28.9 $\pm$ 14.8 Pa with MNPs) as well as the loss modulus (8.1 $\pm$ 4.1 Pa for collagen without MNPs, 8.7 $\pm$ 3.3 Pa with MNPs) were unaffected. Both

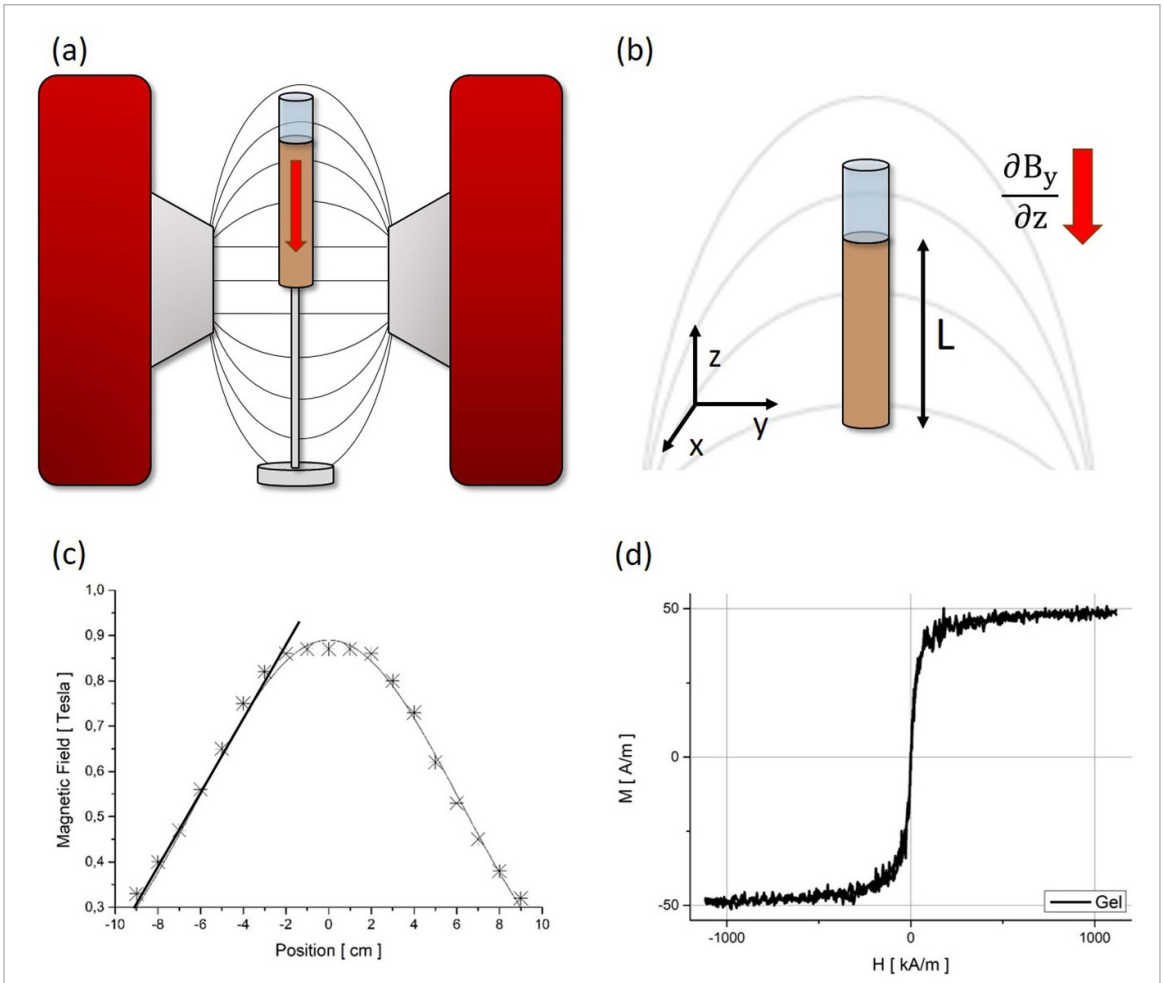

Figure 1. (a) Experimental setup of the magnetic deformation experiments (b) with the mathematical notation of the parameters and (c) strength of the magnetic field of the electromagnet at 96 V as a function of its position. Linear fits were performed on both sides of the curve to determine the strength of the homogeneous field gradient (8 T m^{-1}). The collagen hydrogel with a MNP concentration of 0.5 mg ml^{-1} was prepared in a tubular sample holder with distilled water on top to avoid dehydration. For the deformation experiments, the sample was placed between two magnetic pol shoes in the magnetic field gradient as illustrated in (a) to create a downwards directed magnetic force. To allow magnetic strain, the sample was placed in that field gradient to achieve a difference of approximately 0.32 T from the top to the bottom of the collagen hydrogel. The deformation process was constantly filmed. (d) Hysteresis curve of the MNPs embedded in the collagen hydrogel.

values are in accordance with previously published rheometer analyses of natural and modified collagen hydrogels [22]. Therefore, the mechanical information gained through experiments with magnetically manipulated collagen hydrogels can be transferred to pure *in vitro* generated collagen networks.

Basic cellular viability tests with fibroblasts indicated no toxic effects of the MNPs on the cells (see Appendix, figure A1). Since the MNP are bound inside the network, no hints of cellular uptake from the hydrogel were found in the analysed period of time.

To investigate the magnetic response of this system, a setup in a linear magnetic field gradient was built (figure 1(c)). The collagen hydrogels with incorporated MNP were placed in a tubular sample holder to allow deformation in only one direction.

This construction was placed in a magnetic field gradient created by an electronic magnet and constantly recorded with a digital camera while the downwards directed magnetic force compressed the sample. After 19 h, the collagen samples were turned over in the magnetic field to reverse the magnetic force and to create an upwards directed force to allow an elongation of the deformed sample. The results shown in figures 3(a) and (b) illustrate the normalized compression process, which can be described by

$$y = y_0 e^{-t/\tau} \tag{1}$$

with $y_0 = 1.1$ and $\tau = 4.7$ h, whereas the minimum and maximum gel size is represented by zero and one, respectively.

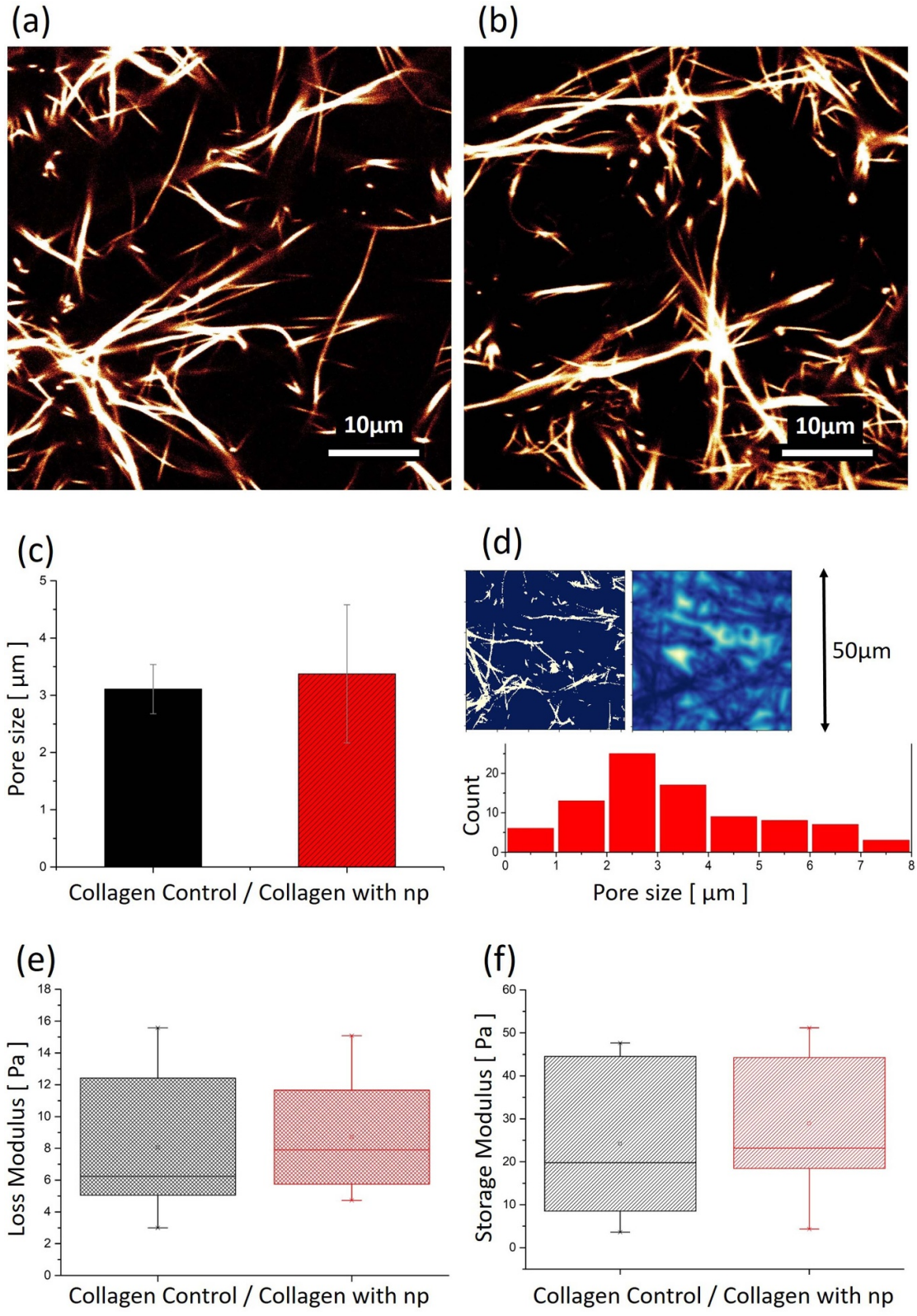

Figure 2. Analysis of the influence of MNP on collagen networks, with a MNP concentration of 0.5 mg ml^{-1}. (a) and (b) Confocal laser-scanning microscopy images of stained collagen hydrogels without (a) and with (b) incorporated MNP. There is no remarkable difference between the hydrogels, the typical network structure remains. (c) Pore size analysis of collagen hydrogels with and without MNP. Both gel-types show no significant difference between the mean pore sizes. (d) Example of pore size analysis process for one stack. The 3D images were binarized and the 3D euclidean distances to the nearest fibre were determined for every voxel. A corresponding distance map with the local maxima representing the centre of a pore was created, whereas the euclidean distance of the local maximum correlates to the pore size of that pore. (e) and (f) Rheological analysis showed no significant difference between loss modulus (e) and storage modulus (f) of collagen hydrogels with and without MNP, respectively. Therefore, no negative influence of the incorporated MNPs on the collagen network could be detected.

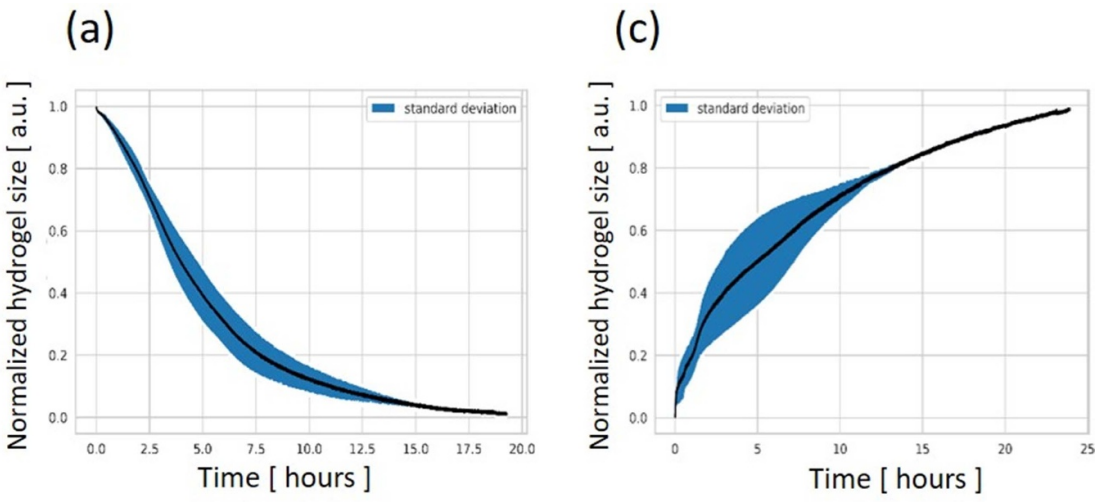

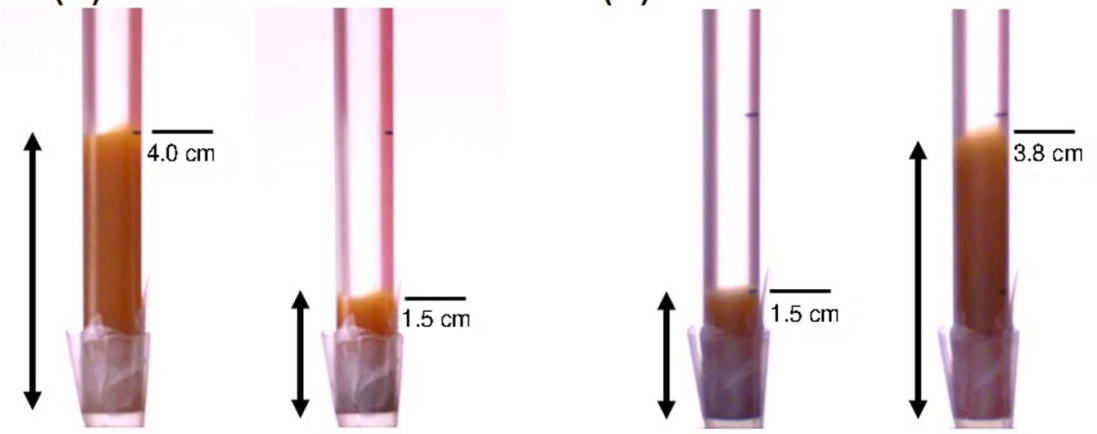

(e)

G	E	C_{11}	M_S	L_0	$\partial B_y/\partial z$	$<\lvert B_y \rvert>$
24.2 Pa	63.8 Pa	90.8 Pa	50 A/m	0.04 m	8 T/m	0.85 T

$\sigma_{zz}^{(a)}$	ΔL^{el}_a	$\sigma_{zz}^{(b)}$	ΔL^{el}_b	$\Delta L^{el}_{a,b}$	σ_{zz}^{*}	ΔL^{*}
8 Pa	0.004 m	21.3 Pa	0.01 m	0.014 m	3.2 Pa	0.0014 m

Figure 3. Illustration of the deformation of collagen hydrogels with 0.5 mg ml^{-1} incorporated MNPs. (a) Normalized process of gel compression over time. This process can be described with the function $y = y_0 e^{-t/\tau}$. Thereby, 1 represents the maximum size of the hydrogel (100%) and 0 the individual minimal size (37.9 ± 4.6%) to normalize the course of the curve for all samples. (b) Pictures before and after the magnetic strain. The collagen hydrogel shrinks to 37.9 ± 4.6% of its original size. The tubular sample holder was completely filled with water to avoid dehydration. (c) Display of the normalized process of gel elongation over time. (d) Pictures before and after the magnetic strain. The collagen hydrogel elongates back to 95.0 ± 0.3% of its original size. Thereby water above the collagen hydrogel was absorbed into the hydrogel to increase the gel size. (e) Prediction of the magnetically induced length changes ΔL^{el} due to force models (a) and (b), respectively, assuming affine elasticity. The generated stresses σ_{zz} clearly exceed the buckling threshold for network collapse σ^*_{zz}. This is in line with the observed experimental length changes ($\Delta L = 0.025$ m) also exceeding the predicted threshold for network collapse $\Delta L^* = \frac{\sigma^*_{zz}}{C_{11}} L_0$.

The deformation achieved in this setup was an average compression of 62 ± 4.6%, compressing the sample to only 38% of its original size (figure 3(b)), while the half-value period is already reached after 3 h. This huge compression enables the collagen hydrogel to release giant amounts of its bound water. Thereby water diffusion is unhindered by the collagen network structure [25]. Without applying a force, this deformation is for the most part irreversible, with only a negligible reversible portion, which corresponds to

other experiments [12, 13]. After moving the compressed collagen sample in the magnetic field into an upwards directed magnetic force, the hydrogel regained 95 ± 0.3% of its original size. This process runs over a 24 h time period, making the size recovery a much slower operation then the compression (figures 3(c) and (d)). With this approach, it was possible to not only compress the collagen hydrogel enormously, but also to revert the resulting deformation. The previously described collagen-collapse [11] can now be induced and gently inverted into a measurable, controllable environment. Consequently, a better understanding of collagen aggregation, fibre interaction and remodelling processes by cells can be achieved providing significant data for further model refinement.

4. Discussion

As for the physics underlying the observed scenario, we first note that our collagen gels reveal connectivities well below the Maxwell isostatic threshold [26], as visible in confocal laser-scanning microscopy measurements (figure 2). Mechanical response thus is not governed by stretching modes, but bending of the fibrils [27] in lieu of other contributions. This particularly holds true, as water has recently been demonstrated to be completely mobile and thus decoupled from network mechanics in similar collagen gels [25]. To relate global and fibril mechanical properties, we first note that similar problems have been the topic of intense research in the hard matter engineering discipline of 'cellular solids' for decades [28]. More precisely, for the reasons mentioned above, our collagen network is expected to behave on formal continuum mechanical basis just as welded stainless steel fibre arrays (basically steel wool) treated by Markaki and Clyne [29]. In this work, the global Young's modulus E and Poisson ratio ν were shown to be

$$E = \frac{9\, E_\mathrm{f}\, f}{32\, (L_\mathrm{f}/D_\mathrm{f})^2},\ \nu = 1/\pi \tag{2}$$

assuming affine deformation in a random network of fibril volume fraction f, fibril length L_f, diameter D_f and Young's modulus E_f, respectively. While the affine deformation regime typically prevails for strains up to some percent, Euler buckling of fibres dominates deformation beyond that, as manifested by increasing strains due to elastic network collapse at a constant plateau stress level [28]

$$\sigma^*_{zz} \approx 0.05\, \frac{8}{3}\, G \tag{3}$$

with shear modulus G.

1 In a first force model, we assume that MNP are homogeneously attached along the collagen fibrils, individually without any coupling, resulting in a ferrogel with an average saturation magnetization M_S. If placed within a heterogenous magnetic field with spatially uniform $\partial B_y/\partial z$ an average magnetic force density

$$f_z = M_\mathrm{s} \frac{\partial B_y}{\partial z} \tag{4}$$

acts on the gel leading to an average stress as large as

$$\sigma^{(\mathrm{a})}_{zz} = \frac{M_\mathrm{S}}{2}\, \frac{\partial B_y}{\partial z} L_0. \tag{5}$$

2 In addition to the model assumptions of uncoupled individual MNP (a), we assume presence of significant magnetic coupling in our second approach that is strong enough to result in magnetic shape anisotropy, viz. dominant preference for magnetization along the fibre axes. It is worth noting here that this assumption can be reconciled with the observed magnetization curves (figure 1(d)) based on the random nature of the network. Within this picture, fibre bending is thus a consequence of the torque exerted on each fibre towards alignment of the fibre axis along the direction of the magnetic field. Following [29] in assuming that the area intersected by an arbitrary plane within a random network equals twice the diameter [30], the average stress contribution on the network is given by

$$\sigma_{zz}^{(\mathrm{b})} = \frac{M_S \left|B_y\right|}{2} \tag{6}$$

In presence of an overall stress σ_{zz}, the average length change for affine deformation within the framework of linear elasticity is given for the present boundary conditions by

$$\Delta L^{\mathrm{el}} = \frac{\sigma_{zz}}{C_{11}} L_0, \text{ where } C_{11} = E\,\frac{1-\nu}{(1-2\nu)(1+\nu)} = G\,\frac{2(1-\nu)}{(1-2\nu)} \tag{7}$$

Figure 3(e) summarizes the predicted stresses for force models (a) and (b), respectively, and the resulting predictions for the length changes within a linear affine elastic framework. Clearly, the predictions of the affine elastic network model for the magnetically induced strains are in the correct order of magnitude, but significantly too low when compared to the experimental observations ($\Delta L = 0.025$ m) for both force models. Estimating the threshold stresses and length changes for network collapse σ_{zz}^* and ΔL^*, respectively, indicate that the experiments are, in fact, performed within the network collapse regime with experimental strains exceeding ΔL^*, and both force models predicting stresses larger than σ_{zz}^*.

As magnetic particle assisted collagen network collapse and recovery was thus demonstrated to be reversible, classification in the framework of viscoelasticity is still desirable. Generally intactness of the network after collapse and recovery hint at elastic collapse [28] due to non-affine network deformation dominated by reversible Euler bucking. Contrarily to the notion of purely elastic collapse, however, strain recovery is not observed after removing the compressive forces, but only after applying restoring forces towards the original sample shape. Also, in the course of collapse, we observe an exponential dependence of deformation on time instead of an instantaneous deformation expected for purely elastic response. While the latter one can be rationalized by the presence of dissipative/viscous contributions originating e.g. due to water within the framework of the Kelvin-Voigt model, the former 'elastic behaviour when applying suitable restoring forces' hints at presence of forces that keep the collagen network in its compressed shape after collapse. We propose that the latter result from local rearrangements/alignments of the collagen side chains resulting in attractive interaction between the fibres in the network (e.g. via electrostatic and hydrophobic interaction or hydrogen bonds) [31]. With increasing density of the network and reorganization processes, that lead to an alignment of fibres under pressure [13], these forces can intensify, hinder the diffusion of water back into the collagen gel and therefore prevent shape recovery. Thus, the applied magnetic forces are necessary to overcome the internal inter-fibril forces that prevent shape recovery after collapse and thus are a measure for the interfibrillar forces in the collapsed state.

5. Conclusions and outlook

To conclude, these experiments show the promising potential of collagen hydrogels with incorporated MNPs as material for biodegradable magnetic responsive systems. No negative impact of MNPs on collagen hydrogel network formation, mechanical properties and cellular viability was observed. Therefore, the resulting highly defined forces could be used for new modelling approaches and mathematical explanations of the manifold usable collagen polymer. Due to their outstanding biocompatibility, collagen hydrogels have great prospects in the field of bioengineering. Being able to reverse compressions on a large scale opens new possibilities to fit the needs of cell culture systems which need mechanical stimuli, e.g. for heart tissue [32]. Furthermore, a biodegradable [33, 34], magnetically responsive bioactuator could be developed with these technical premises.

Acknowledgments

The authors would like to thank Professor Dr Mareike Zink (Leipzig University) for discussion and support as well as Professor Dr Josef Käs (Leipzig University), Dr. Robert Müller (IPHT Jena) for sharing their equipment, Martin Mütze (Leipzig University and IOM) for assistance with rheometer measurements, Marie Deuflhard (Leipzig University and IOM) for constructive discussions and Tom Kunschmann (Leipzig University) for sharing the pore size analysis script. Further, the authors thank Dr U. Müller (Core Unit Durchflusszytometrie CUDZ, College of Veterinary Medicine, University of Leipzig) and Javier Lopez for support with the flow cytometry measurements. This project was funded by the German Research Foundation (DFG), SPP 1681 (MA 2432/6-2 and DU1293/7-3), as well as the German Ministry of Science and Education (BMBF), project EYECULTURE, FKZ 031A574A-C.

Appendix

Table A1. Magnetic properties of the MNPs as powder, dispersed in water and incorporated in the collagen hydrogel.

Sample	M_s in $Am^2\ kg^{-1}$	H_c in $kA\ m^{-1}$	M_r/M_s	c in m-%
Powder	71.42	0.77	0.0227	100
Fluid	1.64	0.35	0.0204	2.30
Gel	0.04	1.02	0.0414	0.06

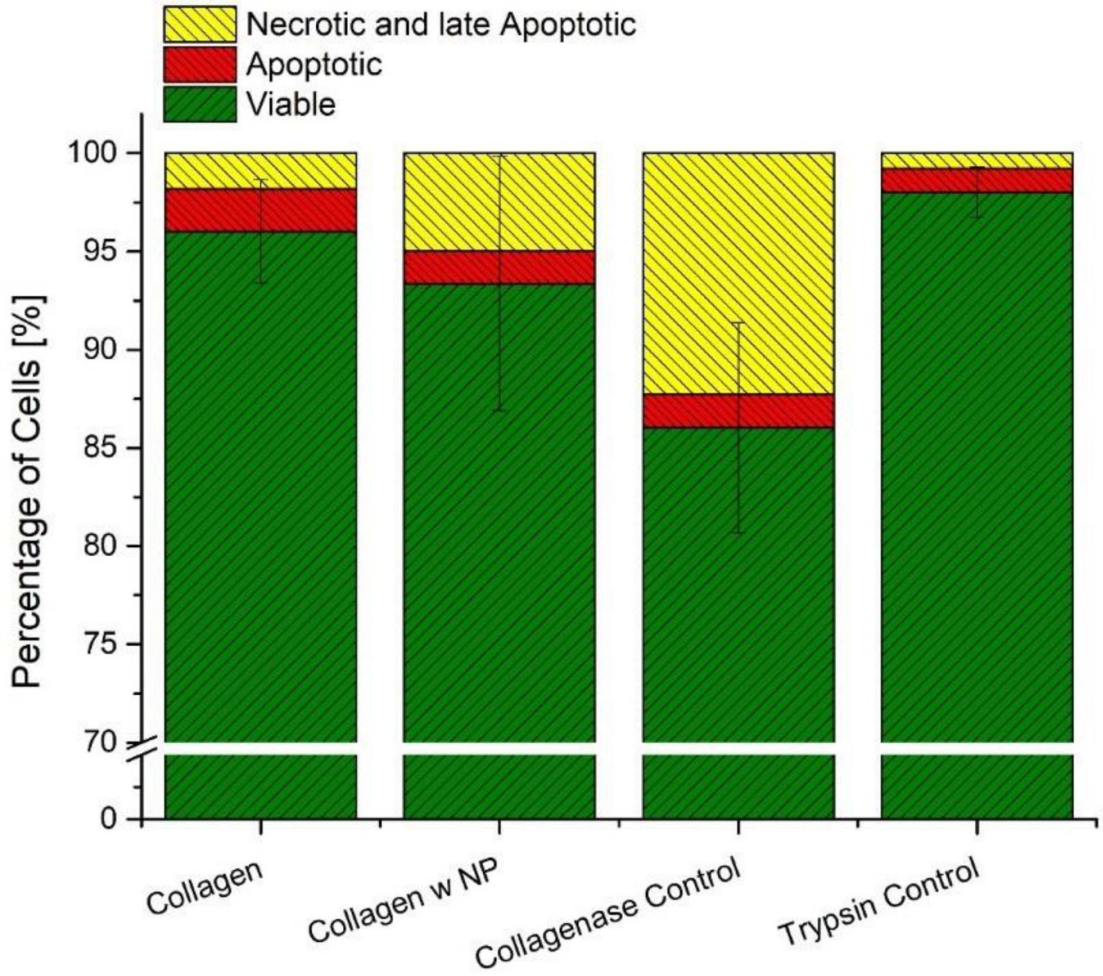

Figure 1. Cellular viability of NIH/3T3 Fibroblasts after 72 h incubation in collagen hydrogels and controls. The protocol is described in detail in Riedel and Hietschold et al [22]. Cells were seeded on collagen gels with and without iron oxide MNPs and on cell culture plates as control. After 72 h the cells were harvested. Control cells from cell culture plates were removed with trypsin (Trypsin Control) or with collagenase (Collagenase Control), to test the toxicity of the removal process. Cells seeded on collagen needed to be removed with collagenase, due to migration processes into the hydrogel. Via propidiumiodide- and annexin-stain and analysis with cell flow cytometry, viable, apoptotic and necrotic and late apoptotic cells were counted. No significant viability loss between collagen with (93.4 ± 6.5) and without (96.0 ± 2.6) iron oxide MNPs was detectable. The collagenase-treatment increases the number of necrotic and late apoptotic cells in comparison to standard trypsin removal.

ORCID iDs

Philine Jauch https://orcid.org/0000-0003-4300-6712
Silvio Dutz https://orcid.org/0000-0002-7258-0943
Stefan G. Mayr https://orcid.org/0000-0002-0969-8738

References

[1] Fratzl P 2008 *Collagen: Structure and Mechanics* 1st edn (Berlin: Springer)

[2] Pedersen J A and Swartz M A 2005 *Ann. Biomed. Eng.* **33** 1469–90
[3] Tibbitt M W and Anseth K S 2009 *Biotechnol. Bioeng.* **103** 655–63
[4] Geckil H, Xu F, Zhang X, Moon S and Demirci U 2010 *Nanomedicine* **5** 469–84
[5] Drury J L and Mooney D J 2003 *Biomaterials* **24** 4337–51
[6] Shoulders M D and Raines R T 2009 *Annu. Rev. Biochem.* **78** 929–58
[7] Janko C, Zaloga J, Pöttler M, Dürr S, Eberbeck D, Tietze R, Lyer S and Alexiou C 2017 *J. Magn. Magn. Mater.* **431** 281–4
[8] Wadajkar A S, Menon J U, Kadapure T, Tran R T, Yang J and Nguyen K T 2013 *Recent Pat. Biomed. Eng.* **6** 47–57
[9] Wang Y-X, Xuan S, Port M and Idee J-M 2013 *CPD* **19** 6575–93
[10] Muthuraman A and Kaur J 2017 Antimicrobial nanostructures for neurodegenerative infections *Nanostructures for Antimicrobial Therapy* (Amsterdam: Elsevier) pp 139–67
[11] Chandran P L and Barocas V H 2004 *J. Biomech. Eng.* **126** 152
[12] Abou Neel E A, Cheema U, Knowles J C, Brown R A and Nazhat S N 2006 *Soft Matter.* **2** 986
[13] Guidry C and Grinnell F 1987 *Coll. Relat. Res.* **6** 515–29
[14] Wen Q and Janmey P A 2013 *Exp. Cell Res.* **319** 2481–9
[15] Dutz S, Andrä W, Hergt R, Müller R, Oestreich C, Schmidt C, Töpfer J, Zeisberger M and Bellemann M E 2007 *J. Magn. Magn. Mater.* **311** 51–54
[16] Weidner A, Gräfe C, von der L M, Remmer H, Clement J H, Eberbeck D, Ludwig F, Müller R, Schacher F H and Dutz S 2015 *Nanoscale Res. Lett.* **10** 992
[17] Kunschmann T, Puder S, Fischer T, Perez J, Wilharm N and Mierke C T 2017 *Biochim. Biophys. Acta, Mol. Cell. Res.* **1864** 580–93
[18] Fischer T, Wilharm N, Hayn A and Mierke C T 2017 *Converg. Sci. Phys. Oncol.* **3** 44003
[19] Paszek M J *et al* 2005 *Cancer Cell* **8** 241–54
[20] Fischer T, Hayn A and Mierke C T 2019 *Sci. Rep.* **9** 8352
[21] Mickel W, Münster S, Jawerth L M, Vader D A, Weitz D A, Sheppard A P, Mecke K, Fabry B and Schröder-Turk G E 2008 *Biophys. J.* **95** 6072–80
[22] Riedel S, Hietschold P, Krömmelbein C, Kunschmann T, Konieczny R, Knolle W, Mierke C T, Zink M and Mayr S G 2019 *Mater. Des.* **168** 107606
[23] Wilharm N, Fischer T, Ott F, Konieczny R, Zink M, Beck-Sickinger A G and Mayr S G 2019 *Sci. Rep.* **9** 12363
[24] Kim J, Feng J, Jones C A R, Mao X, Sander L M, Levine H and Sun B 2017 *Nat. Commun.* **8** 842
[25] Sauer F *et al* 2019 *Soft Matter*
[26] Maxwell J C 1864 *London, Edinburgh, Dublin Philos. Mag. J. Sci.* **27** 294–9
[27] Alexander S 1998 *Phys. Rep.* **296** 65–236
[28] Gibson L J and Ashby M F (eds) 2014 *Cellular Solids* (Cambridge: Cambridge University Press)
[29] Markaki A E and Clyne T W 2005 *Acta Mater.* **53** 877–89
[30] Underwood E E 1970 *Quantitative Stereology (Addison-wesley Series in Metallurgy and Materials)* (Reading, MA: Addison-Wesley)
[31] Nam S, Hu K H, Butte M J and Chaudhuri O 2016 *Proc. Natl Acad. Sci. USA* **113** 5492–7
[32] Govoni M, Muscari C, Guarnieri C and Giordano E 2013 *Biomed. Res. Int.* **2013** 918640
[33] Krane S M 1982 *J. Invest. Dermatol.* **79** 83–86
[34] Aamodt J M and Grainger D W 2016 *Biomaterials* **86** 68–82